

PAPER

Dual-Band Dual-Rectangular-Loop Circular Polarization Antenna for Global Navigation Satellite System

Makoto SUMI^{†a)}, Member and Jun-ichi TAKADA^{††}, Senior Member

SUMMARY This paper proposes a dual-band dual-rectangular-loop circular polarization antenna for Global Navigation Satellite Systems (GNSSs). The proposed antenna combines two large outer rectangular loops with two small inner loops. Each large outer loop is connected to its corresponding small inner rectangular loop. Each loop has gaps located symmetrically with respect to a feed point to produce Right Handed Circular Polarization (RHCP). The gap position and the shape of the rectangular loops are very important to adjust both the impedance matching and circular polarization characteristics. The proposed antenna offers dual-band Voltage Standing Wave Ratio (VSWR) and Axial Ratio (AR) frequency characteristics that include the L1 (1575.42 MHz) and L2 (1227.60 MHz) bands. The antenna gains exceed 8.7 dBi. Broad AR elevation patterns are obtained. These antenna characteristics are well suited to precise positioning.

key words: dual-band, circular polarization, rectangular loop with a gap, GNSS, precise positioning

1. Introduction

The demand for precise positioning using Global Navigation Satellite Systems (GNSSs) has recently increased. There is a wide range of fields where highly accurate measurements are required such as surveying, civil engineering construction, agriculture, crustal deformation research, earthquake prediction, construction and mining machines, and cultivator machines. For autonomous agricultural vehicles, real time centimeter-accurate positioning is required [1]. Some available systems are the United States' Global Positioning System (GPS), Russia's GLObal NAVigation Satellite System (GLONASS), and the European Union's Galileo. In addition, China's Compass (Beidou) and Japan's Quasi-Zenith Satellite System (QZSS) were launched in 2012 and 2010, respectively. GNSSs are expected to be fully deployed and operational in a few years. According to [2], multi-constellation features can increase the availability, accuracy, integrity, and robustness of GNSSs. Furthermore, [2] states that nearly 70% of GNSS receivers remain single-frequency (with the remaining 20% supporting two and 10% supporting three frequencies). The most common combination for the GNSS receivers that support multiple frequencies is the L1 and L2 frequencies. All GNSS receivers use the L1 frequency. Approximately 30% of the receivers have L2

capability, and 10% have L5. Recently, multi-frequency capability has become common to achieve high precision. The benefits of supporting multiple frequencies include improved accuracy and robustness. Recently, a dual-frequency capability including the L1 band (1575.42 MHz) and the L2 band (1227.60 MHz) has become necessary to satisfy high-accuracy requirements. In the future, a triple-frequency capability will almost certainly become necessary [2], [3]. Therefore, the demand is high for GNSS antennas that can support multiple frequencies.

Generally, Circular Polarization (CP) antennas can be roughly classified into two types. The first type is the antenna derived from linearly polarized antennas that have functions for radiating CP. Some examples of this are a cross-dipole antenna with a phase difference of 90 deg. [4], cross-dipole antenna that adopts the perturbation technique [5], patch antennas to which perturbation elements are added [6], antennas using a polarization converter [7], [8], and sequential arrays [9]. There are some cases among these where the feeding method is complicated or the phase center is shifted. The second type is an antenna that has structures for CP such as an axial-mode helix antenna [10] and spiral-like antennas [10]–[12]. These antennas can be classified as traveling wave antennas.

On the other hand, some CP antennas comprising loops with gaps were proposed in [12]–[17]. These report on one-loop-structure and two-loop-structure antennas. One-loop-structure antennas were reported in [12] and [13]. Two-loop-structure antennas were reported in [14]–[16]. Since all of these antennas use a ground plane, it is considered that they have a high affinity with the metal body of a vehicle. The maximum beam direction of the one-loop structure antennas with gaps tends to shift from the zenith due to their asymmetrical antenna structure. Conversely, the maximum beam direction of the two-loop structure antennas with gaps tends to be the zenith due to their symmetrical antenna structures. All antennas are based on traveling waves and their Axial Ratio (AR) frequency characteristics are greater than 12% (≤ 3 dB). However, the investigations on the antennas proposed in [13] and [15] do not consider impedance matching. The antennas in [14] and [16] require impedance transformers or broadband baluns for impedance matching. Most of these antennas have a relatively high antenna gain. In particular, the two-loop-structure antennas achieve a gain greater than 8 dBi. The antenna in [16] exhibits a high azimuth dependency of elevation patterns on the frequency due to its long rectangular structure. A slot antenna comprising two rectangular

Manuscript received February 8, 2019.

Manuscript publicized June 25, 2019.

[†]The author is with the Wireless Emerging Technology Group, Research Laboratories, NTT DOCOMO, Inc., Yokosuka-shi, 239-8536 Japan.

^{††}The author is with the School of Environment and Society, Tokyo Institute of Technology, Tokyo, 152-8552 Japan.

a) E-mail: sumi@ieec.org

DOI: 10.1587/transcom.2019EBP3043

loop slots with a cavity was developed in [17], however, the antenna requires a cavity. Therefore, it is considered that it would be difficult to install this antenna into the flat metal body of a vehicle.

Members of our research group proposed a configuration of two rectangular wire loops fed in series for broadband circular polarization and impedance matching [18]. Each rectangular loop is connected to each end of a feed element. The two gap positions on the loops are set symmetrically with respect to the center of the antenna to radiate CP. The antenna achieved good broadband Voltage Standing Wave Ratio (VSWR) and AR frequency characteristics with a single feed at the same time. Loop antennas comprising parasitic elements were proposed to broaden the bandwidth [15], [16], [19]. The small inner loops are driven by currents on large outer loops. The details on the loop antennas comprising parasitic elements are given in [19]. This technique is similar to that of parasitic dipole antennas [20], [21]. This paper proposes a new dual-band dual-rectangular-loop CP antenna and targets GNSS applications. We added new small inner loops inside the large outer loops. This structure is based on the previously proposed antenna in [18] and we connect the inner loops to the outer loops in order to achieve operation in dual bands including the L1 and L2 bands. The multi-band technique of the proposed antenna structure is similar to that of a multi-branch dipole [22], [23]. Frequency characteristics are analyzed using the FEKO electromagnetic simulator (Ver.7.0.2, EMSS) [24] based on the Method of Moments.

The rest of this paper is organized as follows. First, the dual-band CP antenna design concept and preliminary design for the proposed antenna are described in Sect. 2. The VSWR and AR frequency characteristics and the current distributions are shown. Second, the proposed antenna structure to which a dielectric substrate is applied is described in Sect. 3. The frequency characteristics for the VSWR and AR, radiation patterns, and AR elevation patterns are presented. Third, investigation results on the operating mechanism of the proposed antenna are given in Sect. 4. We focus on the center frequencies for the VSWR and AR while changing the antenna parameters. The impact of the antenna parameters on the center frequencies and the frequency design procedure are described. Finally, our conclusions are given in Sect. 5.

2. Preliminary Design of Dual-Band Antenna

Our target frequency bands are defined in Table 1. In this section, the low and high bands are defined as the L2 band (1227.60 MHz) and the L1 band (1575.42 MHz), respectively. Figure 1 shows a dual-band CP antenna design concept based on the previously proposed antenna in [18]. Figures 1(a) and 1(b) show design concepts for the low- and high-band antennas, respectively. These antennas have two gapped rectangular loops. Each rectangular loop is connected to each end of a feed element. The two gap positions on the loops are set symmetrically with respect to the center of the antenna to radiate CP. Figure 1(c) shows a combina-

Table 1 Target frequency.

Band	Frequency
Low band	1227.60 MHz (L2 band)
High band	1575.42 MHz (L1 band)

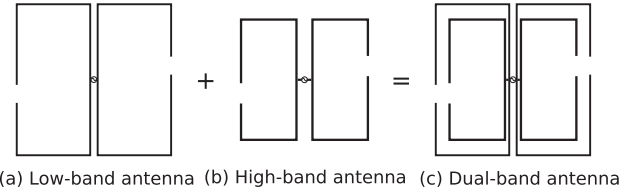


Fig. 1 Antenna design concept.

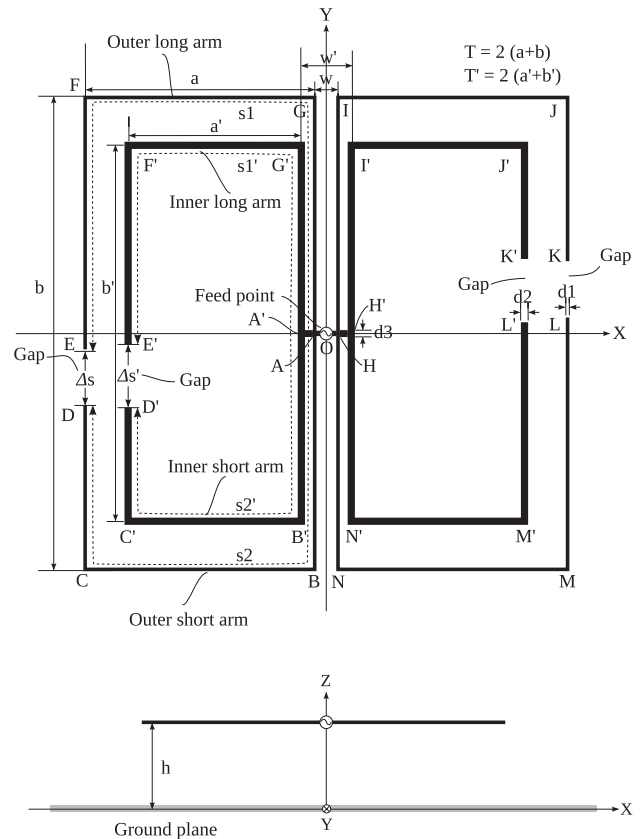


Fig. 2 Preliminary design of dual-band antenna ($h = 53.5$ mm, $T = 2(a+b) = 376.4$ mm, $T' = 2(a'+b') = 294.6$ mm, $a = 61.5$ mm, $b = 126.7$ mm, $a' = 46.4$ mm, $b' = 100.9$ mm, $a/b = 0.485$, $a'/b' = 0.460$, $w = 6.4$ mm, $w' = 13.4$ mm, $s1 = 193$ mm, $s1' = 150.3$ mm, $s2 = 169$ mm, $s2' = 127.3$ mm, $\Delta s = 14.4$ mm, $\Delta s' = 17$ mm, $d1 = 1$ mm, $d2 = 2$ mm, and $d3 = 2$ mm).

tion of the large loop and the small loop to achieve operation in the dual bands.

Figure 2 shows the preliminary design for the proposed dual-band CP antenna. The optimal parameters are shown in Fig. 2. The antenna has two large outer rectangular loops of the same size (E-F-G-A-B-C-D and L-M-N-H-I-J-K) and two small inner loops of the same size (E'-F'-G'-A'-B'-C'-D' and L'-M'-N'-H'-I'-J'-K'). The side lengths of the outer large rectangular loops are a and b , a' and b' , respectively. The

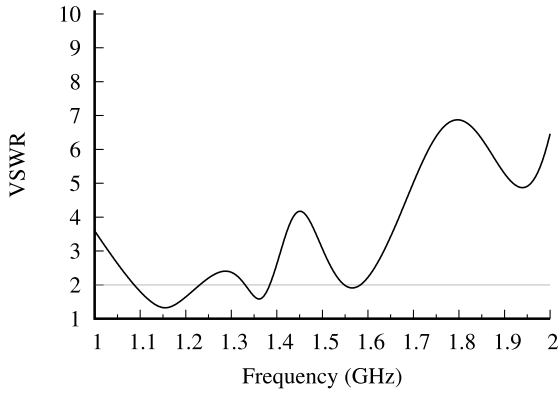


Fig. 3 VSWR frequency characteristics.

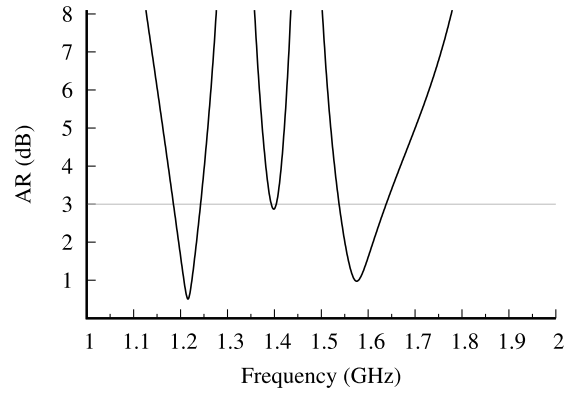


Fig. 4 AR frequency characteristics.

circumferences are $T (= 2(a+b))$ and $T' (= 2(a'+b'))$. Each large outer rectangular loop is connected to each end of the feed element (A-O-H) with length w separating them. Each small inner rectangular loop is connected to each connecting point (A' or H') of each large outer loop and the end of the feed element. Each large outer rectangle has a gap with widths of Δs at the distances s_1 and s_2 from the point (A or H) connected to the feed element. Each small inner rectangle has a gap with widths of $\Delta s'$ at the distances s_1' and s_2' from the point (A' or H') connected to each large outer rectangle loop. These gaps are located symmetrically with respect to the feed point to produce Right Handed Circular Polarization (RHCP) for GNSSs in the low and high bands. The antenna is placed above a 600×600 mm ground plane. The antenna height is determined by an approximately intermediate value of 0.25 wavelengths between the low and high bands. The loop surface is parallel to the ground plane.

2.1 VSWR Frequency Characteristics

Figure 3 shows the VSWR frequency characteristics. The antenna achieves operation in the dual bands including the low and high bands. The VSWR bandwidth (≤ 2) including the low band is 12.4%, and the VSWR bandwidth (≤ 2) including the high band is 2.1%.

2.2 AR Frequency Characteristics

Figure 4 shows the AR frequency characteristics. The antenna achieves operation in the dual bands including the low and high bands. The AR bandwidth (≤ 3 dB) including the low band is 4.8%, and the AR bandwidth (≤ 3 dB) including the high band is 6.3%. As described in Sect. 3, RHCP is obtained in the low and high bands. Based on these investigation results, the preliminary design achieves operation in the dual bands including the low and high bands.

2.3 Current Distributions

First, we focus on the left outer and inner loops in Fig. 2. Figures 5 and 6 show the current distributions in the low and high bands, respectively.

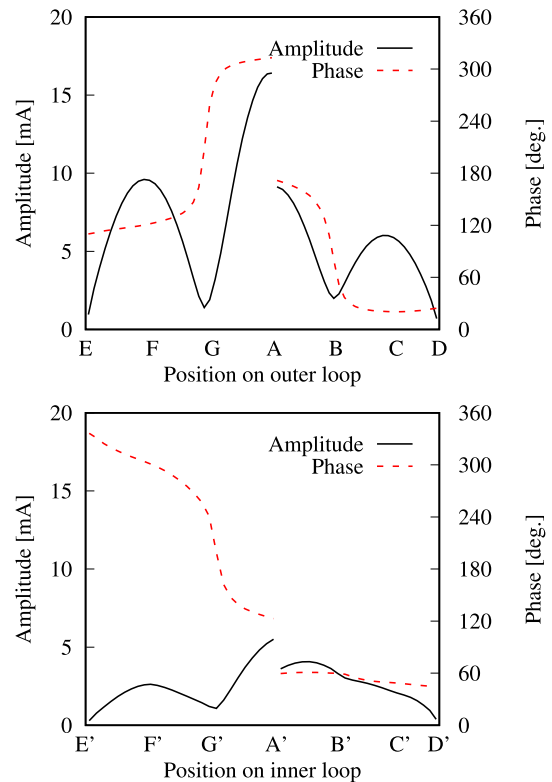


Fig. 5 Current distribution in low band.

Two standing waves on segments G-F-E and D-C-B are observed. The phase difference between these currents on segments G-F-E and D-C-B is approximately 90 deg. Similarly, two standing waves on segments (G'-F'-E' and D'-C'-B') are observed. The phase difference between these currents on segments (G'-F'-E' and D'-C'-B') is approximately 90 deg. Most of the radiation in the low band comes from corners F and C on the outer loop, and most of the radiation in the high band F' and C' on the inner loop. This tendency is the same in the right loop with corners J and M in the low band, and corners J' and M' in the high band. In addition, these corners on the left loops are 180 deg. out of phase at the corresponding corners on the left loops because the structure is symmetrical with respect to the center of the

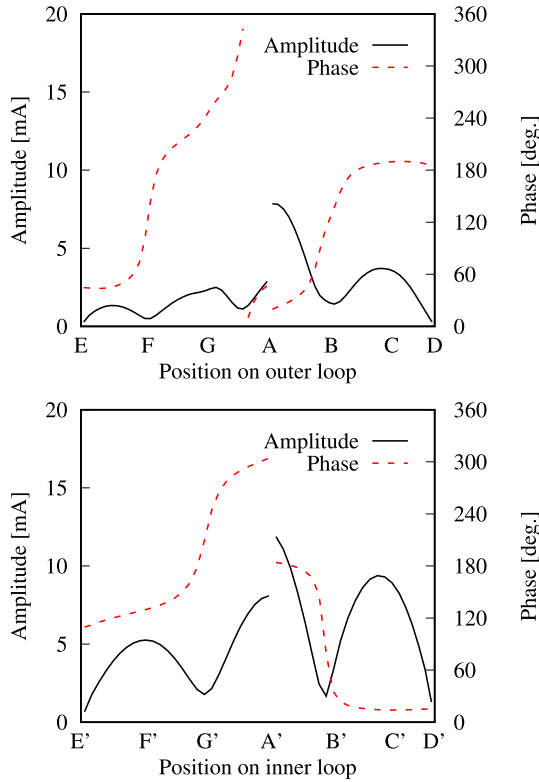


Fig. 6 Current distribution in high band.

antenna. Therefore, the CP radiation is produced by the sequential 90 degree rotation of the corner geometry and the 90 degree phase difference with each 90 degree rotation of the corner.

It is considered that segment B-A-G does not contribute to radiation since it forms a transmission line with segment N-H-I. Similarly, segment B'-A'-G' does not contribute to radiation since it forms a transmission line with segment N'-H'-I'. The RHCP wave is mainly radiated from the outer loop except for segment B-A-G in the low band. Similarly, the RHCP wave is mainly radiated from the inner loop except for segment B'-A'-G' in the high band.

Furthermore, we consider that the circular polarization waves can be easily switched from RHCP to Left Handed Circular Polarization (LHCP) waves by replacing the positions of the gaps using Micro Electro Mechanical Systems (MEMS) or PIN-diodes.

3. Proposed Antenna Structure

Figure 7 shows the proposed antenna structure with a dielectric substrate for mass production. This structure is based on the preliminary design in Sect. 2. The optimal parameters are shown in Fig. 7. The antenna is placed above a 600×600 mm ground plane. The antenna height adopts an approximately intermediate value of 0.25 wavelengths between the low and high bands. The loop surface is parallel to the ground plane.

The prototype antenna shown in Fig. 8 is constructed from a printed circuit board (dielectric constant = 3.3, thick-

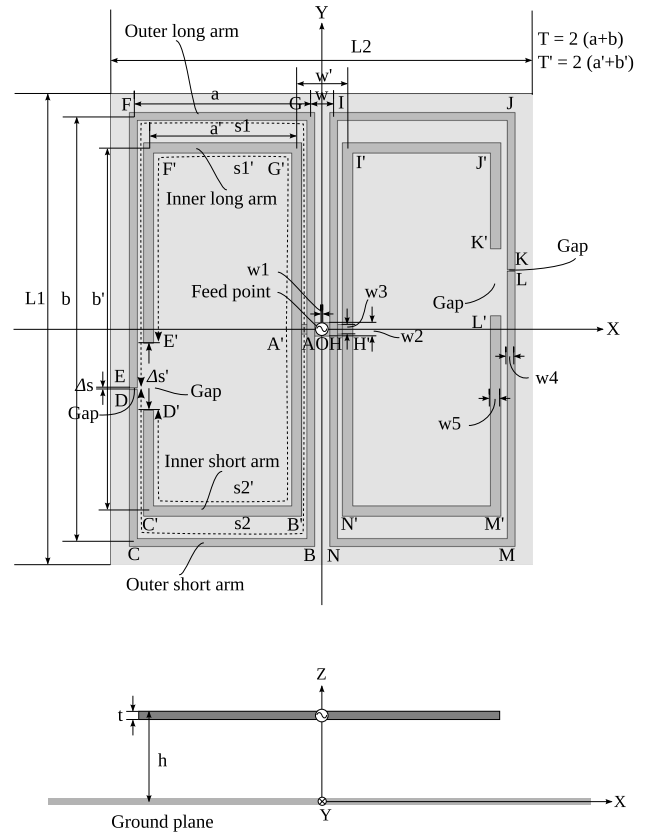


Fig. 7 Proposed antenna structure ($\epsilon_r = 3.3$, $t = 1.6$ mm, $h = 51.7$ mm, $L1 = 102.6$ mm, $L2 = 91.8$ mm, $T = 2(a+b) = 262$ mm, $T' = 2(a'+b') = 222$ mm, $a = 38.4$ mm, $b = 92.6$ mm, $a' = 32.1$ mm, $b' = 78.9$ mm, $a/b = 0.415$, $a'/b' = 0.407$, $w = 5$ mm, $w' = 11$ mm, $s1 = 143.7$ mm, $s1' = 128.5$ mm, $s2 = 118$ mm, $s2' = 78.9$ mm, $\Delta s = 0.3$ mm, $\Delta s' = 14.6$ mm, $w1 = 0.3$ mm, $w2 = 3$ mm, $w3 = 2$ mm, $w4 = 1.7$ mm, and $w5 = 2.2$ mm).

ness = 1.6 mm, CS-3376C, Risyo Kogyo Co. LTD., Japan) using a substrate processing machine. The antenna board is supported by styrene foam.

3.1 VSWR Frequency Characteristics

Figure 9 shows the VSWR frequency characteristics of the numerical and measured results. The antenna achieves operation in the dual bands including the low and high bands. The VSWR bandwidth (≤ 2) including the low band is 16.0%, and the VSWR bandwidth (≤ 2) including the high band is 7.4% based on calculation.

3.2 AR Frequency Characteristics

Figure 10 shows the AR frequency characteristics of the numerical and measured results. The antenna achieves operation in the dual bands including the low and high bands. The AR bandwidth (≤ 3 dB) including the low band is 5.0%, and the AR bandwidth (≤ 2) including the high band is 5.3% based on calculation. The VSWR and AR frequency characteristics have two resonance characteristics including the L1 and L2 bands. When the results for the previously proposed antenna in [18] and those for the proposed antenna in

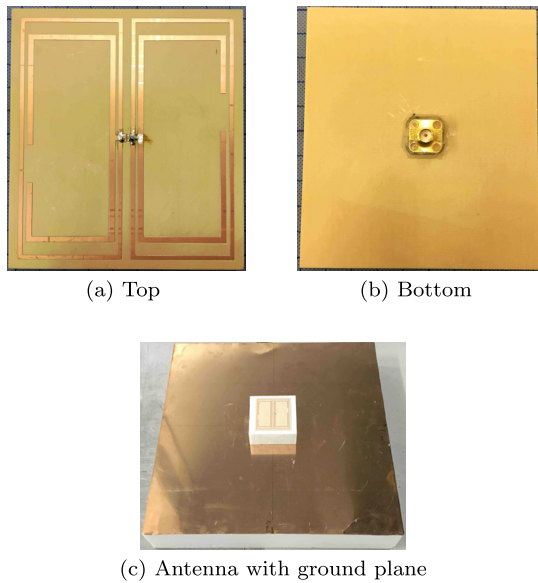


Fig. 8 Prototype antenna.

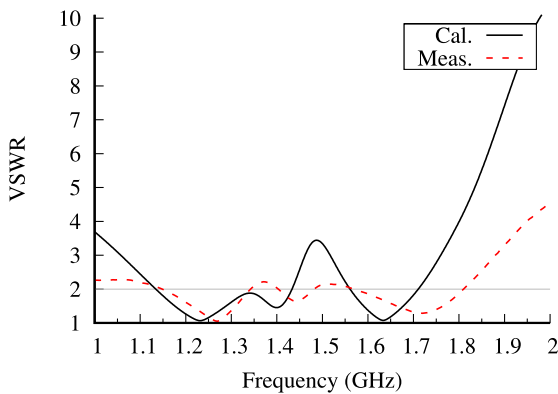


Fig. 9 VSWR frequency characteristics for the numerical and measured results.

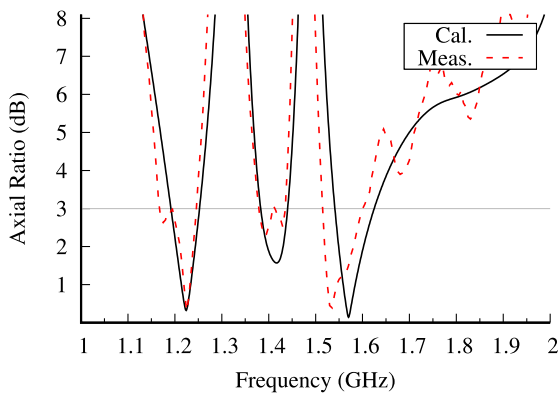
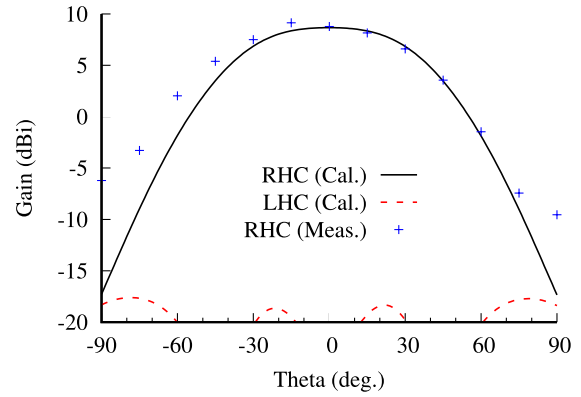
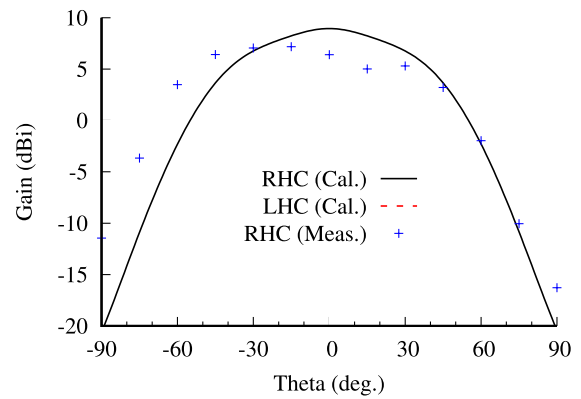


Fig. 10 AR frequency characteristics for the numerical and measured results.

Fig. 7 are compared, the frequency characteristics have been changed from broadband to two resonances. However, for GNSS antennas, it is considered that the receiving antennas



(a) 1.227 GHz



(b) 1.575 GHz

Fig. 11 Radiation patterns in YZ-plane for the numerical and measured results.

should not have broadband but multiband frequency characteristics. If the antenna receives only the desired bands, the circuits on the RF front end side can be simplified. It is considered that the frequency characteristics of the proposed antenna function as a kind of Band-Pass Filter (BPF).

3.3 Radiation Patterns

Figures 11 and 12 show the numerical and measured radiation patterns in the YZ- and ZX-planes, respectively. The maximum radiation direction is obtained at the zenith in the low and high bands. In the case of a 1-loop CP antenna, the maximum radiation direction deviates slightly from the zenith direction due to their asymmetrical structures [12], [13]. The proposed 2-loop-structure radiates RHCP in the zenith direction due to the symmetrical structure. The numerical and measured antenna gains for RHCP at 1.227 GHz are 8.7 dBi and 9.2 dBi, respectively. The numerical and measured antenna gains for RHCP at 1.575 GHz are 8.9 dBi and 7.2 dBi, respectively. The antenna efficiency becomes 93.6% at 1.227 GHz and 93.5% at 1.575 GHz, respectively, based on calculation.

3.4 AR Elevation Patterns

Figures 13 and 14 show the numerical and measured AR

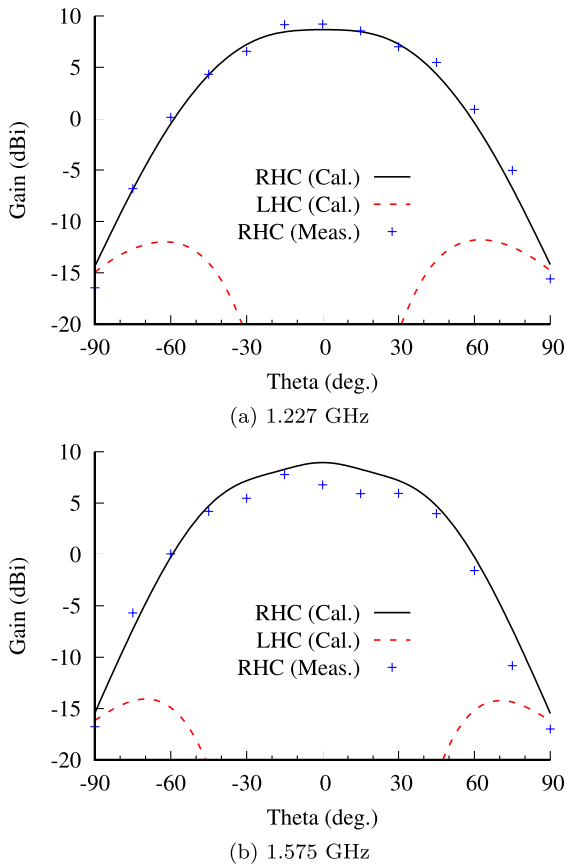


Fig. 12 Radiation patterns in ZX-plane for the numerical and measured results.

elevation patterns in the YZ- and ZX-planes, respectively. The angles from the zenith are used to describe the AR elevation patterns. Although the range in the ZX-plane in the low band is slightly narrower than the others, the AR (≤ 3 dB) can be achieved roughly in the range from $\theta = -60$ deg. to $\theta = 60$ deg. Broad AR elevation patterns are obtained.

Generally, the cut off angle, θ_c , for terrestrial applications is expected to be approximately $50^\circ > \theta_c > 70^\circ$. The AR of < 3 dB or the cross polarization (LHCP) of < -10 dB is desired over $\theta < \theta_c$ for GNSS antennas. In addition, $G_{\min} > -10$ dBic for RHCP is required to provide a sufficient signal-to-noise ratio (SNR) for detection [3]. The proposed antenna meets these specifications.

The measured and numerical results exhibit the similar tendencies. There is a slight difference between the numerical and experimental results. The differences are due to the different conditions of the feed point between the numerical and measured models, manufacturing error, measurement equipment, and measurement error. A delta-gap feed is used for calculation and a SMA connector without a balun is used for the measurement. In the future, some tuning will be required for commercialization.

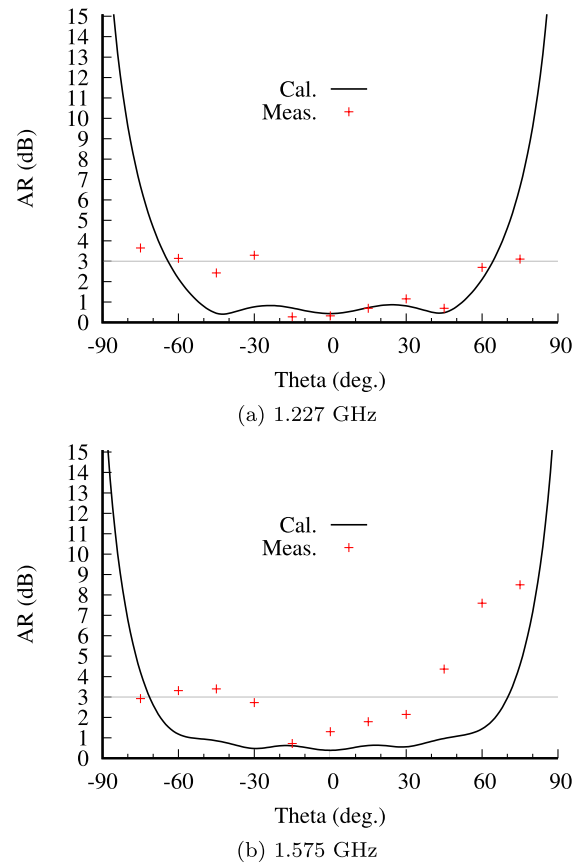


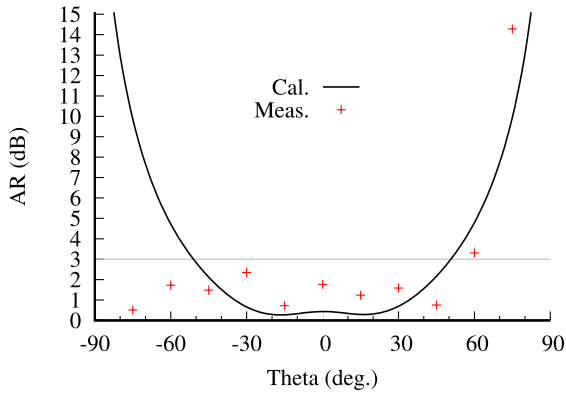
Fig. 13 Axial ratio elevation patterns in YZ-plane for the numerical and measured results.

4. Investigation of Operating Mechanism

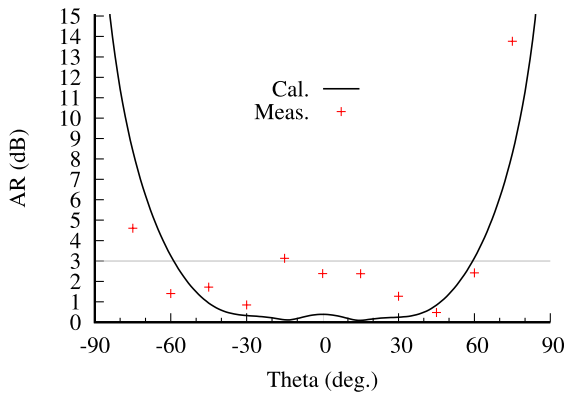
4.1 Difference in Characteristics between 1-Loop Structures and 2-Loop Structure

Figure 15 shows the 1-loop structures (outer loop and inner loop) and the 2-loop structure based on the proposed antenna in Fig. 7. Figures 16 and 17 show the VSWR and AR frequency characteristics, respectively. The VSWR center frequency of the outer loop in the low band is close to that for the 2-loop structure. The VSWR center frequency of the inner loop in the high band is almost the same as that for the 2-loop structure. On the other hand, the AR center frequency of the outer loop in the low band is slightly higher than that for the 2-loop structure. The AR center frequency of the inner loop in the high band is higher than that for the 2-loop structure. There are a few differences between the 1-loop and 2-loop structures.

The proposed antenna is designed using the following procedure. First, the center frequencies of the VSWR in the low and high bands are adjusted by changing each loop size. Second, the center frequencies of the AR in the low and high bands are adjusted by changing each parameter carefully. For the 2-loop structure, the outer loop and the inner loop affect each other. This trend is especially apparent in the



(a) 1.227 GHz



(b) 1.575 GHz

Fig. 14 Axial ratio elevation patterns in ZX-plane for the numerical and measured results.



(a) Low-band antenna (b) High-band antenna (c) Dual-band antenna

Fig. 15 1-loop structures (outer loop and inner loop) and 2-loop structure (combination of outer and inner loops).

high band. Therefore, parametric studies are conducted in order to clarify the influence of the shape of each element on the center frequency in Sect. 4.2.

4.2 Influence of Antenna Parameters on VSWR and AR Frequency Characteristics

The influence of the antenna parameters on the VSWR and AR characteristics is investigated. In this investigation, one antenna parameter in Fig. 7 is changed at a time. The other antenna parameters are shown in Fig. 7. In addition, the edge ratios, a/b and a'/b' , are fixed and the perimeter length is changed based on changes in the antenna parameters. In these parametric studies, we focus on the center frequencies of the VSWR and AR. The center frequency of the VSWR

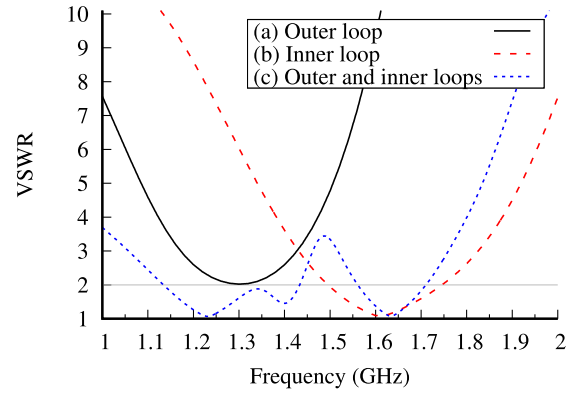


Fig. 16 VSWR frequency characteristics for inner loop, outer loop, and combined configuration.

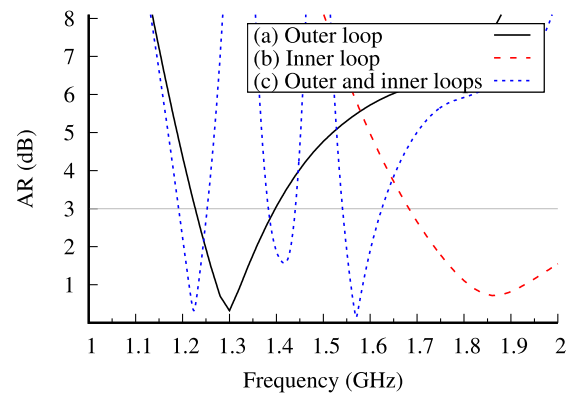


Fig. 17 AR frequency characteristics for inner loop, outer loop, and combined configuration.

is defined as the frequency when the reactance component of the impedance becomes zero. The center frequency of the AR is defined as the frequency when the AR becomes minimal.

4.2.1 Influence of Long Arm Length on Outer and Inner Loops, s_1 and s_1'

Figure 18 shows the relationship between the center frequency and the long arm length when distance s_1 from point A or H is varied from 139.7 mm to 163.7 mm in 2 mm steps and distance s_1' from point A' or H' is varied from 114.5 mm to 134.5 mm in 2 mm steps. In these parametric studies, the symbols, $VSWR_{low}$, $VSWR_{high}$, AR_{low} , and AR_{high} are defined as the center frequencies of the VSWR in the low band, the VSWR in the high band, the AR in the low band, and the AR in the high band, respectively.

4.2.2 Influence of Short Arm Length on Outer and Inner Loops, s_2 and s_2'

Figure 19 shows the relationship between the center frequency and the short arm length when distance s_2 from point A or H is varied from 113 mm to 143 mm in 5 mm steps and distance s_2' from point A' or H' is varied from 58.9 mm to

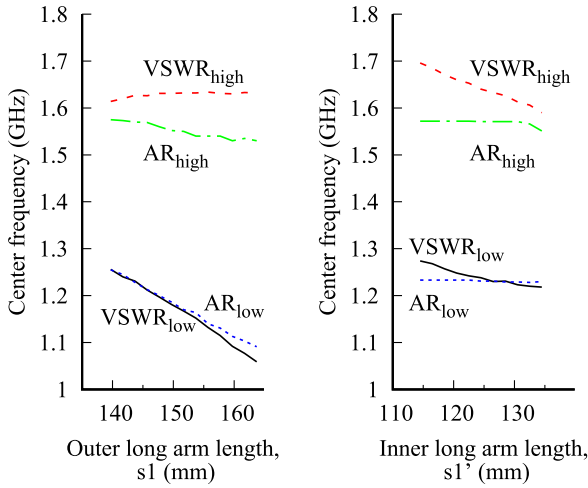


Fig. 18 Effect of long arm length on VSWR and AR.

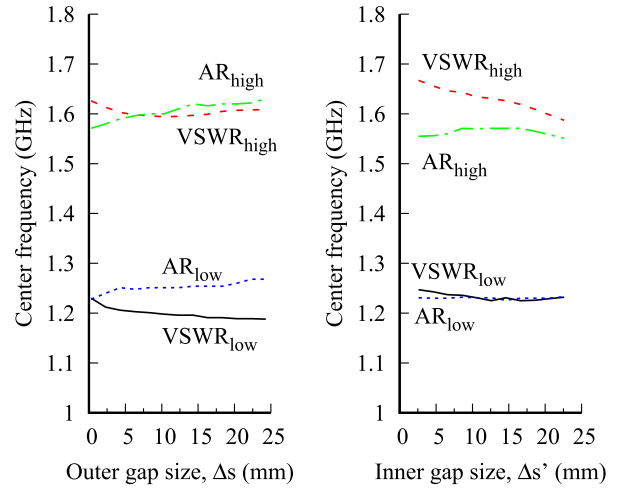


Fig. 20 Effect of gap size on VSWR and AR.

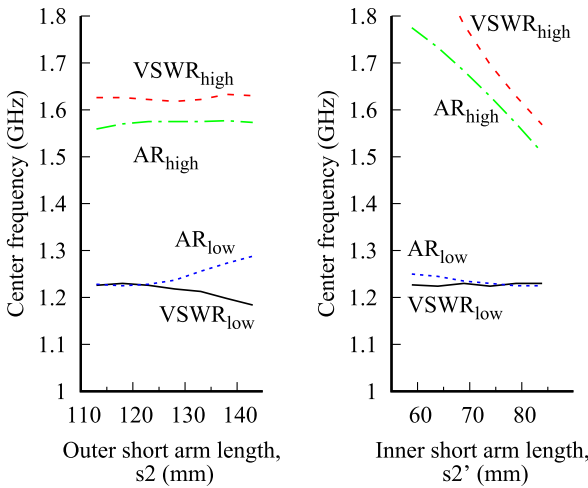


Fig. 19 Effect of short arm lengths on VSWR and AR.

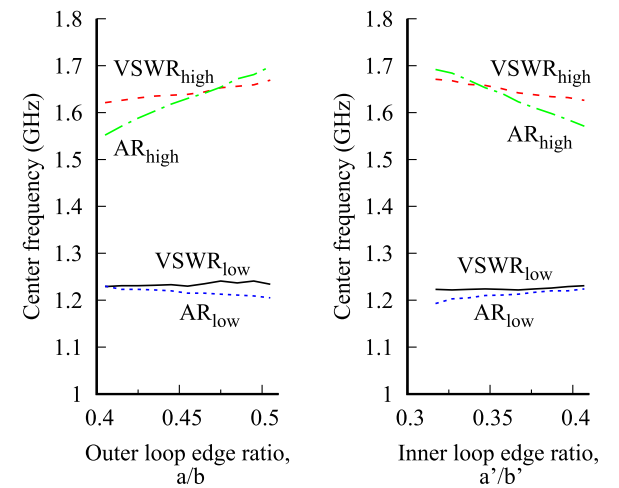


Fig. 21 Effect of edge ratio on VSWR and AR.

83.9 mm in 5 mm steps.

4.2.3 Influence of Gap Size on Outer and Inner Loops, Δs and $\Delta s'$

Figure 20 shows the relationship between the center frequency and the gap size when the gap size in the outer loop, Δs , is varied from 0.3 mm to 24.3 mm in 2 mm steps and the gap size in the inner loop, $\Delta s'$, is varied from 2.6 mm to 22.6 mm in 2 mm steps.

The investigations on the long arm lengths, the short arm lengths, and the gap sizes are organized hereafter.

4.2.4 Influence of Edge Ratio of Loops, a/b and a'/b'

Figure 21 shows the relationship between the center frequency and the edge ratio of the outer and inner loops when the edge ratio of the outer loop, a/b , is varied from 0.405 to 0.505 in 0.01 steps and the edge ratio of the inner loop, a'/b' , is varied from 0.317 to 0.407 in 0.01 steps. As shown

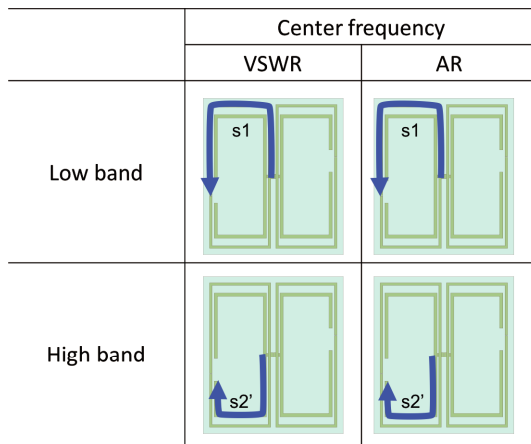
in Figs. 16 and 17, the outer loop and the inner loop affect each other in the 2-loop structure. When edge ratio a/b is decreased or edge ratio a'/b' is increased, the spacing between the inner and outer loops becomes larger. In this case, the spacing represents the distance between B-C (I-J) and B'-C' (I'-J'), or that between G-F (N-M) and G'-F' (N'-M'). In the proposed 2-loop configuration, when the spacing between the inner and outer loops becomes wider in the high band, both the outer and inner loops are used and the entire antenna loop size becomes larger. Therefore, it is considered that the AR center frequency in the high band becomes lower.

4.3 Impact of Antenna Parameters on Center Frequencies and Frequency Design Procedure

The influence of each antenna parameter on the center frequency is shown in Figs. 18–20. The fitting functions are adopted to clarify the difference in the influence on the center frequency for each parameter. The center frequency curves are fitted by linear functions to find the frequency

Table 2 Antenna parameters and center frequencies.

Parameter	Impact on center frequency (MHz/mm)			
	VSWR _{low}	VSWR _{high}	AR _{low}	AR _{high}
Outer long arm, s1	↓↓ -8.3	- 0.6	↓↓ -7.0	- -2.1
Inner long arm, s1'	- -2.8	↓ -5.0	- -0.3	- -0.6
Outer short arm, s2	- -1.5	- 0.2	- 2.2	- 0.4
Inner short arm, s2'	- 0.2	↓↓↓↓ -16.7	- -1.1	↓↓↓ -10.7
Outer gap size, Δs	- -1.4	- -0.2	- 0.9	- 2.2
Inner gap size, Δs'	- -0.8	↓ -3.6	- 0.0	- 0.0
	0–2.9: -, 3.0–5.9: ↓ or ↑, 6.0–8.9: ↓↓ or ↑↑ 9.0–11.9: ↓↓↓ or ↑↑↑, 12.0+: ↓↓↓↓ or ↑↑↑↑			

**Fig. 22** Elements that strongly affect the center frequency.

trends. Table 2 shows the relationship between the antenna parameters and the center frequencies. When each parameter is increased, the changes in the center frequencies are indicated in units of megahertz/millimeters (MHz/mm) in Table 2. The number of arrows in Table 2 shows the impact on the center frequencies. More arrows represent a stronger impact. An upward pointing arrow, ↑, indicates that the frequency becomes high, and a downward pointing arrow, ↓, indicates that the frequency becomes lower. The elements that have a strong influence on the center frequencies are organized in 22. From these parametric studies, we find that the shape of the outer long arms (E-F-G-A and L-M-N-H) has a great impact on the center frequencies of the VSWR and AR in the low band. Similarly, the shape of the inner short arms (A'-B'-C'-D' and H'-I'-J'-K') has a great impact on the center frequencies of the VSWR and AR in the high band. Therefore, based on these investigations, each element should be adjusted.

5. Conclusion

We proposed a dual-band dual-rectangular-loop circular polarization antenna for GNSSs. The proposed antenna offers dual-band operation including the L1 and L2 bands. The

VSWR bandwidth (≤ 2) including the low band is 16.0%, and the VSWR bandwidth (≤ 2) including the high band is 7.4%. The AR bandwidth (≤ 3 dB) including the low band is 5.0%, and the AR bandwidth (≤ 3 dB) including the high band is 5.3%. Furthermore, the impact of the antenna parameters on the center frequencies and that on the frequency design procedure were shown. The proposed antenna radiates RHCP in the dual bands using a symmetrical structure with respect to the feed point. Investigations on current distributions showed that CP waves are generated by the sequential 90 degree rotation of the corner geometry and the 90 degree phase difference with each 90 degree rotation of the corner. The antenna gains in RHCP of 8.7 dBi in the low band and 8.9 dBi in the high band were obtained. The proposed antenna meets general radiation pattern specifications for terrestrial GNSS applications. Broad AR elevation patterns were obtained. Therefore, the proposed antenna is suited to precise positioning using GNSSs. Three frequency capability supporting L5 (1176.45 MHz) is a topic for further study.

Acknowledgments

The authors sincerely thank Prof. Kazuhiro Hirasawa of the University of Tsukuba for his illuminating discussions.

References

- [1] J.C. del Rey, J.A. Vega, M. Pérez-Ruiz, and L. Emmi, "Comparison of positional accuracy between RTK and RTX GNSS based on the autonomous agricultural vehicles under field conditions," *Appl. Eng. Agric.*, vol.30, no.3, pp.361–366, 2014.
- [2] European Global Navigation Satellite Systems Agency, "2016 GNSS User Technology Report," 2016.
- [3] J.J. Wang, "Antennas for Global Navigation Satellite System (GNSS)," *Proc. IEEE*, vol.100, no.7, pp.2349–2355, 2012.
- [4] S.X. Ta, I. Park, and R.W. Ziolkowski, "Crossed dipole antennas: A review," *IEEE Antennas Propag. Mag.*, vol.57, no.5, pp.107–122, 2015.
- [5] M.F. Bolster, "A new type of circular polarizer using crossed dipoles," *IRE Trans. Microw. Theory Techn.*, vol.9, no.5, pp.385–388, Sept. 1961.
- [6] M. Haneishi, S. Yoshida, and N. Goto, "A broadband microstrip array composed of single-feed type circularly polarized microstrip antennas," *Antennas and Propagation Society International Symposium*, 1982, pp.160–163, IEEE, 1982.
- [7] M. Chen and G. Tsandoulas, "A wide-band square-waveguide array polarizer," *IEEE Trans. Antennas Propag.*, vol.21, no.3, pp.389–391, 1973.
- [8] M.J. Franco, "A high-performance dual-mode feed horn for parabolic reflectors with a stepped-septum polarizer in a circular waveguide [antenna designer's notebook]," *IEEE Antennas Propag. Mag.*, vol.53, no.3, pp.142–146, June 2011.
- [9] T. Teshirogi, M. Tanaka, and W. Chujo, "Wideband circularly polarized array antenna with sequential rotations and phase shift of elements," *Microstrip Antennas: The Analysis and Design of Microstrip Antennas and Arrays*, p.136, Wiley-IEEE Press, 1995.
- [10] J.D. Kraus and R.J. Marhefka, *Antenna for All Applications*, McGraw Hill, Upper Saddle River, NJ, 2002.
- [11] H. Nakano, S. Okuzawa, K. Ohishi, H. Mimaki, and J. Yamauchi, "A curl antenna," *IEEE Trans. Antennas Propag.*, vol.41, no.11, pp.1570–1575, 1993.

- [12] R.L. Li, V.F. Fusco, and H. Nakano, "Circularly polarized open-loop antenna," *IEEE Trans. Antennas Propag.*, vol.51, no.9, pp.2475–2477, 2003.
- [13] H. Morishita, K. Hirasawa, and T. Nagao, "A circularly polarized broadband rhombic loop antenna," *IEICE Trans. Commun.*, vol.E79-B, no.6, pp.865–870, 1996.
- [14] Y. Zhang and L. Zhu, "Printed dual spiral-loop wire antenna for broadband circular polarization," *IEEE Trans. Antennas Propag.*, vol.54, no.1, pp.284–288, 2006.
- [15] H. Morishita, K. Hirasawa, and T. Nagao, "Circularly polarised wire antenna with a dual rhombic loop," *IEE Proc., Microw. Antennas Propag.*, vol.145, no.3, pp.219–224, 1998.
- [16] R. Li, S. Basat, A. Traille, J. Laskar, and M. Tentzeris, "Development of wideband circularly polarised square-and rectangular-loop antennas," *IEE Proc., Microw. Antennas Propag.*, vol.153, no.3, pp.293–300, 2006.
- [17] S. Shi, K. Hirasawa, and Z.N. Chen, "Circularly polarized cavity backed two-element rectangular loop slot antenna," *IEICE Trans. Electron.*, vol.E82-C, no.7, pp.1217–1222, July 1999.
- [18] M. Sumi, K. Hirasawa, and S. Shi, "Two rectangular loops fed in series for broadband circular polarization and impedance matching," *IEEE Trans. Antennas Propag.*, vol.52, no.2, pp.551–554, 2004.
- [19] R. Li, G. DeJean, J. Laskar, and M.M. Tentzeris, "Investigation of circularly polarized loop antennas with a parasitic element for bandwidth enhancement," *IEEE Trans. Antennas Propag.*, vol.53, no.12, pp.3930–3939, 2005.
- [20] J.M. Floc'h and H. Rmili, "Design of multiband printed dipole antennas using parasitic elements," *Microw. Opt. Technol. Lett.*, vol.48, no.8, pp.1639–1645, 2006.
- [21] R.J. Coe and M.S. Morse, "Dipole antenna with parasitic elements," US Patent 4,812,855, March 14 1989.
- [22] Z. Ying, "Multiple band, multiple branch antenna for mobile phone," US Patent 6,329,962, Dec. 11 2001.
- [23] D. Liu, "A multi-branch monopole antenna for dual-band cellular applications," *IEEE Antennas and Propagation Society International Symposium. 1999 Digest. Held in conjunction with: USNC/URSI National Radio Science Meeting (Cat. no.99CH37010)*, pp.1578–1581 vol.3, July 1999.
- [24] Altair, Engineering, INC., "FEKO EM simulation software," [Online]. Available: <http://www.feko.info/>



Jun-ichi Takada (S'89–M'93–SM'11) received the B.E., M.E., and D.E. degrees from the Tokyo Institute of Technology, Tokyo, Japan, in 1987, 1989, and 1992, respectively. He was a Research Associate with Chiba University, Chiba, Japan, from 1992 to 1994. He was an Associate Professor with the Tokyo Institute of Technology from 1994 to 2006, and is currently a Full Professor at the Institute. From 2003 to 2007, he also served as a Researcher with the National Institute of Information and Communications Technology, Tokyo, Japan. His current research interests include radio-wave propagation and channel modeling for mobile and short range wireless systems, regulatory issues of spectrum sharing, and ICT applications for international development. Dr. Takada has been appointed as a fellow of the Institute of Electronics, Information, and Communication Engineers (IEICE) since 2012. He received the IEICE Achievement Award in 2008.



Makoto Sumi received the B.S. degree in electrical engineering from Meiji University, Japan, in 1999, the M.S. degree in electrical engineering from the University of Tsukuba, Japan, in 2001, and the Ph.D. degree in international development engineering from the Tokyo Institute of Technology, Japan, in 2018, respectively. He is a researcher with the wireless emerging technology research group, Research Laboratories, NTT DOCOMO, INC., Japan. His current research interests are the design of small antennas

for mobile communications and M2M applications, circular polarization antennas for GNSS/GPS, metamaterial antennas, and antenna measurement techniques. He received the Young Researcher Award of the Institute of Electronics, Information, and Communication Engineers (IEICE) Technical Committee on Antennas and Propagation in 2009. He is a member of the IEEE and the IEICE.